Enhancement of glass-forming ability of FeCoNiBSiNb bulk glassy alloys with superhigh strength and good soft-magnetic properties

Baolong Shen[a] and Chuntao Chang
Institute for Materials Research, Tohoku University, Sendai 980-8577, Japan

Zhefeng Zhang
Shenyang National Laboratory for Materials Science, Institute of Metal Research, Chinese Academy of Sciences, Shenyang 110016, China

Akihisa Inoue
Institute for Materials Research, Tohoku University, Sendai 980-8577, Japan

(Received 16 December 2006; accepted 6 June 2007; published online 19 July 2007)

The effect of Zr addition on the glass-forming ability (GFA) of FeCoNiBSiNb glassy alloys in $[(Fe_{0.6}Co_{0.3}Ni_{0.1})_{0.75}B_{0.2}Si_{0.05}]_{96-x}Nb_4Zr_x$ system was investigated. In addition to slight increases of glass transition temperature from 818 to 822 K and supercooled liquid region from 60 to 65 K, the 1 at. % Zr addition was found to be effective in approaching alloy to a eutectic point as well as decreasing liquidus temperature from 1427 to 1400 K, resulting in an increase in GFA. By copper mold casting, $[(Fe_{0.6}Co_{0.3}Ni_{0.1})_{0.75}B_{0.2}Si_{0.05}]_{95}Nb_4Zr_1$ bulk glassy alloys (BGAs) with diameters in the range up to 6 mm were produced. The BGA exhibits a superhigh fracture strength of 4180 MPa, and Young's modulus of 200 GPa, combined with an elastic strain of 0.02. The glassy alloy exhibits good soft-magnetic properties as well, i.e., rather high saturation magnetization of 1.1 T, low coercive force of 2 A/m, and high permeability of 16 700 at 1 kHz under a field of 1 A/m. The reason why only 1 at. % Zr is effective in improving GFA and the fracture mechanisms during compression of this Fe-based BGA were discussed. © *2007 American Institute of Physics*. [DOI: 10.1063/1.2757013]

I. INTRODUCTION

Since amorphous alloys in Fe-metalloid system were found to exhibit good soft-magnetic properties in 1974,[1–3] a large number of studies on the development of soft-magnetic amorphous alloys have been carried out for the subsequent 20 years. However, the shape and dimension of the Fe-based amorphous magnetic alloys had been limited to thin ribbon form with thicknesses below almost 30 μm due to the necessity of a high cooling rate of almost 10^6 K/s for formation of an amorphous phase.[4] By devoting subsequent great efforts, a distinct glass transition before crystallization was found in $Fe_{72}Al_5Ga_2P_{11}C_6B_4$ alloy, and an $Fe_{73}Al_5Ga_2P_{11}C_5B_4$ ferromagnetic bulk glassy alloy (BGA) was synthesized in 1995.[5,6] Since then, a variety of Fe-based ferromagnetic BGAs has been developed because of their potential magnetic applications.[7–9] The development of Fe- and Co-based BGAs with high glass-forming ability (GFA) has attracted increasing interest due to a high potential for applications as structural[10–16] and functional (ferromagnetic)[17–25] materials. These Fe- and Co-based BGAs can be classified into two groups. One group was developed by Ponnambalam *et al.*[11] and Lu *et al.*,[12] respectively, by adding small amounts of Y or Er to previously reported FeCrMoBC BGAs,[26] as Y or Er can improve the manufacturability of these alloys by scavenging the oxygen impurity from them via the formation of innocuous Y or Er oxides. The other one is an FeBSi-based BGA group developed by Inoue *et al.*,[13] without any Ln (lanthanides) element additions, just improving the stability of the supercooled liquid through adjusting the alloy compositions. Nevertheless, the Y, or Er-containing Fe-based glassy alloys that can be cast into glassy alloy rods with diameters up to 12 mm exhibit paramagnetic properties at room temperature, and the problem of extreme brittleness remains unresolved. On the other hand, for the FeBSi-based BGA group, although they exhibit good soft-magnetic properties at room temperature and outstanding mechanical properties,[18] the GFA is not so high compared to the Y, or Er-containing Fe-based glassy alloys, which is not sufficient yet even for the applications as soft-magnetic materials used for magnetic parts such as valves, clutches, or relays.

In this study, with the aim of synthesizing an FeBSi-based BGA with much high GFA, and simultaneously exhibiting superhigh fracture strength and good soft-magnetic properties, we examined the effect of Zr addition on the improvement of GFA, as it has been proven to be effective in improving the GFA of FeBSi-based BGAs.[27] The $[(Fe_{0.6}Co_{0.3}Ni_{0.1})_{0.75}B_{0.2}Si_{0.05}]_{96}Nb_4$ alloy was chosen a base alloy, because this alloy exhibited a large supercooled liquid region of 60 K in FeCoNiBSi glassy alloy system,[28] which means that the thermal stability of the supercooled liquid is high for this alloy.[29]

II. EXPERIMENT

Multicomponent Fe-based alloy ingots with compositions of $[(Fe_{0.6}Co_{0.3}Ni_{0.1})_{0.75}B_{0.2}Si_{0.05}]_{100-x}Zr_x$ ($x=0-3$) and $[(Fe_{0.6}Co_{0.3}Ni_{0.1})_{0.75}B_{0.2}Si_{0.05}]_{96-x}Nb_4Zr_x$ ($x=0-2$) were pre-

[a]Electronic mail: shen@imr.tohoku.ac.jp

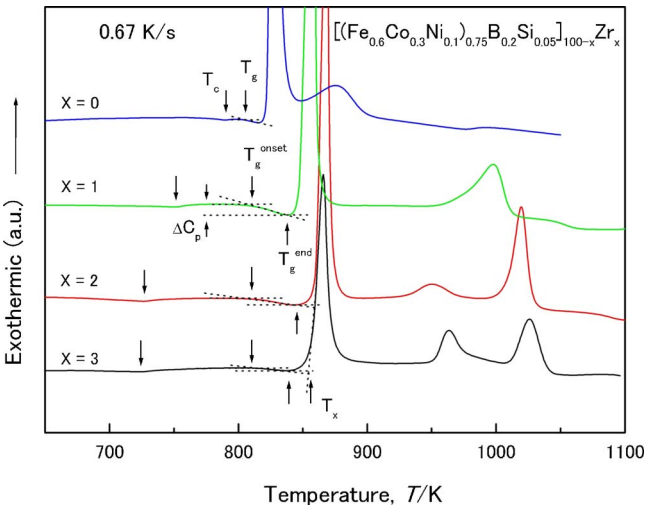

FIG. 1. (Color online) DSC curves of melt-spun $[(Fe_{0.6}Co_{0.3}Ni_{0.1})_{0.75}B_{0.2}Si_{0.05}]_{100-x}Zr_x$ (x=0, 1, 2, and 3) glassy alloy ribbons.

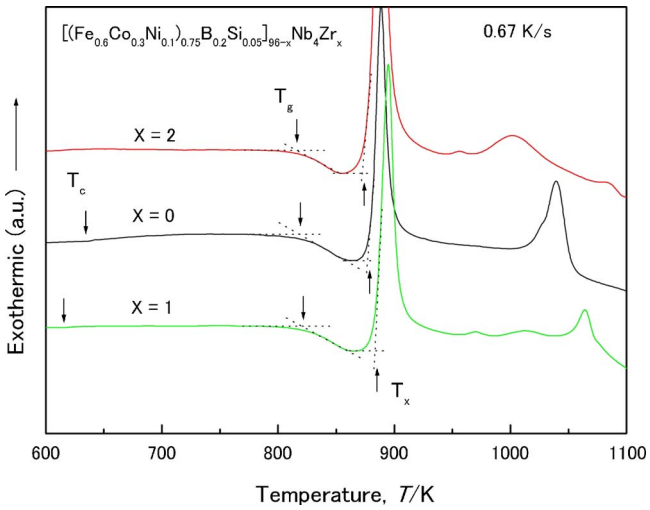

FIG. 2. (Color online) DSC curves of melt-spun $[(Fe_{0.6}Co_{0.3}Ni_{0.1})_{0.75}B_{0.2}Si_{0.05}]_{100-x}Nb_4Zr_x$ (x=0, 1, and 2) glassy alloy ribbons.

pared by arc melting the mixtures of pure Fe, Co, Ni, Nb, and Zr metals and pure B and Si crystals in an argon atmosphere. The alloy compositions represent nominal atomic percentages. Bulk glassy alloy rods with diameters of 2–7 mm were produced by the ejection copper mold casting method. Glassy alloy ribbons with a cross section of 0.02 $\times 1.2$ mm^2 were also produced by the melt spinning method. The glassy structure was identified by x-ray diffraction (XRD), and the absence of micrometer scale crystalline phase was examined by optical microscopy. Thermal stability associated with glass transition temperature (T_g), crystallization temperature (T_x), supercooled liquid region ($\Delta T_x = T_x - T_g$), and Curie temperature (T_C) was examined by differential scanning calorimetry (DSC) at a heating rate of 0.67 K/s. The melting (T_m) and liquidus (T_l) temperatures were measured with a differential thermal analyzer (DTA). The heating rate used was 0.67 K/s. Mechanical properties of Young's modulus (E), compressive fracture strength (σ_f), and elastic strain (ε) were measured with an Instron testing machine. The gauge dimension was 2 mm in diameter and 4 mm in length, and the strain rate was 5×10^{-4} s^{-1} for the 4 mm sample. Deformation and fracture behaviors were examined by scanning electron microscopy (SEM). Saturation magnetization (I_s) was measured with a vibrating sample magnetometer. Coercive force (H_c) was measured with a *B-H* loop tracer under a field of 800 A/m. Effective permeability (μ_e) up to 100 kHz was measured with an impedance analyzer under a field of 1 A/m.

III. RESULTS

First, we examined the effect of Zr on improvement for thermal stability of the supercooled liquid of the $[(Fe_{0.6}Co_{0.3}Ni_{0.1})_{0.75}B_{0.2}Si_{0.05}]_{100-x}Zr_x$ glassy alloys to optimize Zr content. Figure 1 shows DSC curves of the $[(Fe_{0.6}Co_{0.3}Ni_{0.1})_{0.75}B_{0.2}Si_{0.05}]_{100-x}Zr_x$ (x=0, 1, 2, and 3) glassy alloys produced by melt spinning. It is clearly seen that the distinguished glass transition appears only in the 1 at. % Zr-containing alloy. The onset and end temperatures of glass transition are marked as T_g^{onset} and T_g^{end}, respectively. For these glassy alloys, it is seen that the difference of specific heat (ΔC_p) between the onset and the end of glass transition increases largely with adding 1 at. % Zr, and then decreases with further increasing Zr content from 1 to 3 at. %. The value of ΔC_p at the glass transition region (i.e., between temperature ranges of T_g^{onset} and T_g^{end}) indicates how much different the structure changes are at the glass transition.[30] Thus, it is considered that the thermal stability of the supercooled liquid increases with only 1 at. % Zr addition. With increasing Zr content to 3 at. %, the glass transition almost disappears. In addition, although the crystallizations for the 0 and 1 at. % Zr-containing alloys take place through two exothermic stages, the two corresponding exothermic peaks are located closely for the 0 at. % Zr-containing alloy, while the two corresponding exothermic peaks are located distantly for the 1 at. % Zr-containing alloy. The further increasing Zr content from 1 to 2 or 3 at. % causes the three-stage crystallization. Therefore, it is suggested that just 1 at. % Zr addition is effective in improving the thermal stability of the supercooled liquid in this alloy system. However, even for this alloy, it cannot be cast into glassy alloy rod with the diameter larger than 3 mm, being attributed to its smaller ΔT_x of 35 K, which is not enough for preparing Fe-based BGA rods with diameters larger than 3 mm. Otherwise, it is also seen from the DSC curves that T_C decreases largely by adding Zr, which is attributed to the *s* electrons from Zr elements occupying the 3*d* bands of Fe and Co elements. The low T_C causes a decrease in I_s.

According to the results obtained above, we tried to add only 1 or 2 at. % Zr in $[(Fe_{0.6}Co_{0.3}Ni_{0.1})_{0.75}B_{0.2}Si_{0.05}]_{96}Nb_4$ glassy alloy with the aim of synthesizing an Fe-based BGA rod with diameters larger than 5 mm, combined with the rather high I_s. Figure 2 shows DSC curves of the $[(Fe_{0.6}Co_{0.3}Ni_{0.1})_{0.75}B_{0.2}Si_{0.05}]_{96-x}Nb_4Zr_x$ (x=0, 1, and 2) glassy alloys produced by melt spinning. It is also seen that only 1 at. % Zr addition is effective in enlarging ΔT_x from 60 to 65 K. With increasing Zr content to 2 at. %, ΔT_x decreases from 60 to 55 K. T_g increases slightly from 818 to 822 K by adding 1 at. % Zr as well, but decreases

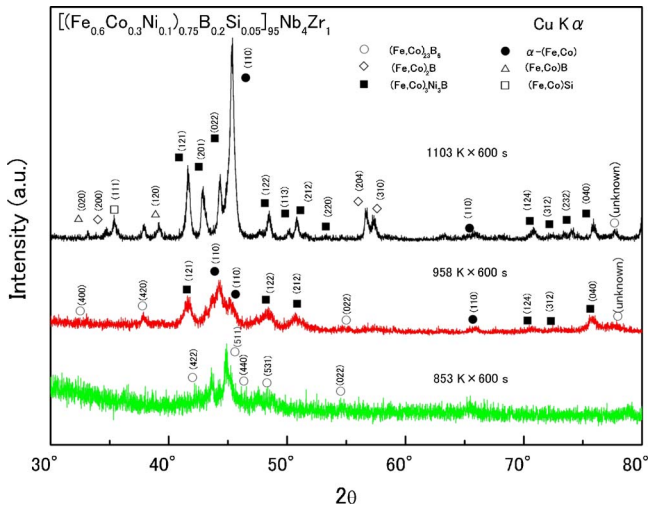

FIG. 3. (Color online) XRD patterns of the $[(Fe_{0.6}Co_{0.3}Ni_{0.1})_{0.75}B_{0.2}Si_{0.05}]_{95}Nb_4Zr_1$ glassy alloy samples annealed for 60 s at 853 K and for 600 s at 958 and 1098 K.

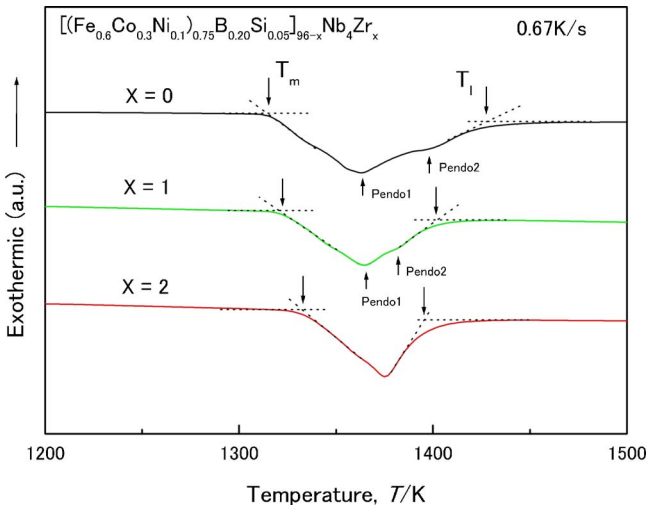

FIG. 4. (Color online) DTA curves of $[(Fe_{0.6}Co_{0.3}Ni_{0.1})_{0.75}B_{0.2}Si_{0.05}]_{100-x}Nb_4Zr_x$ (x=0, 1, and 2) alloys.

from 822 to 815 K with further increasing Zr content from 1 to 2 at. %. Besides, the temperature interval between the two exothermic peaks increases by adding 1 at. % Zr but decreases with a further increase of Zr content to 2 at. %. It is therefore suggested that the thermal stability of the supercooled liquid against crystallization increases with 1 at. % Zr addition but begins to decrease with a further increase of Zr content. Here, it is seen that T_C either decreases with increasing Zr content. The T_C of the 0 and 1 at. % Zr-containing alloys are 635 and 616 K, respectively, but the T_C of the 2 at. % Zr-containing alloy is below 600 K, as shown in the DSC curves.

The crystallization behavior of the $[(Fe_{0.6}Co_{0.3}Ni_{0.1})_{0.75}B_{0.2}Si_{0.05}]_{95}Nb_4Zr_1$ glassy alloy was investigated by XRD measurement. Figure 3 shows XRD patterns of this glassy alloy subjected to annealing for 600 s at 853 K, which is between T_g and T_x, and 600 s at 958 and 1103 K, corresponding to the temperatures just above the first and the second exothermic peaks, respectively, as shown in Fig. 2. The XRD patterns are identified as a complex fcc $(Fe,Co)_{23}B_6$ phase for the sample annealed at 853 K. It is therefore confirmed that the primary precipitation phase of this glassy alloy system is an $(Fe,Co)_{23}B_6$ metastable phase, which is consistent with the former results obtained from the Fe- and Co-based BGAs.[31–33] The primary precipitation of the $Fe_{23}C_6$-type phase having a complex fcc structure with a large lattice parameter of 1.12 nm including 96 atoms[34] from the networklike glassy structure requires long-range atomic rearrangements of constituent elements, leading to the high stability of the supercooled liquid against crystallization.[35]

We also investigated the melting behavior of this alloy system. Figure 4 shows DTA curves of the $[(Fe_{0.6}Co_{0.3}Ni_{0.1})_{0.75}B_{0.2}Si_{0.05}]_{96-x}Nb_4Zr_x$ (x=0, 1, and 2) alloys. For the 0 at %Zr-containing alloy, two endothermic peaks marked as P_{endo1} and P_{endo2} can be seen although P_{endo2} peak is small, implying that the composition does not lie in a eutectic point despite lying in the vicinity of that point. By adding 1 at. % Zr, the P_{endo2} peak becomes weak, and the T_l decreases from 1427 to 1400 K, combined with the decrease of temperature interval between T_m and T_l from 112 to 78 K. With further increasing Zr content to 2 at. %, the peak P_{endo2} disappears completely, and the temperature interval between T_m and T_l decreases from 98 to 64 K, implying that the composition of the alloy approaches a eutectic point with increasing Zr content. Therefore, it is considered that except for behaving the highest thermal stability of the supercooled liquid in this alloy system, the $[(Fe_{0.6}Co_{0.3}Ni_{0.1})_{0.75}B_{0.2}Si_{0.05}]_{95}Nb_4Zr_1$ alloy lies in the vicinity of a eutectic point. Besides, its reduced glass transition temperature (T_g/T_l) is 0.587 (822/1400). All of these results obtained from the DSC, XRD, and DTA measurements mean that the $[(Fe_{0.6}Co_{0.3}Ni_{0.1})_{0.75}B_{0.2}Si_{0.05}]_{95}Nb_4Zr_1$ alloy exhibits high GFA combined with a high T_C.

Consequently, we tried to form cylindrical glassy alloy rods for the $[(Fe_{0.6}Co_{0.3}Ni_{0.1})_{0.75}B_{0.2}Si_{0.05}]_{95}Nb_4Zr_1$ alloy and its critical diameter was 6 mm. Their as-cast surfaces all appear smooth and lustrous. No apparent volume reductions can be recognized on their surfaces, indicating that there was no drastic crystallization during the formation of these samples. Figure 5 shows XRD patterns of the cast alloy rods with diameters of 4, 5, and 6 mm. Only broad peaks without a crystalline peak can be seen for all of these bulk samples, indicating the formation of a glassy phase in the diameter range up to 6 mm. The DSC examination results also denote the formation of a glassy phase. The XRD and DSC measurement results indicate clearly the formation of the Fe-based glassy alloy rods with diameters in the range up to 6 mm. Here we want to emphasize that such an Fe-based ferromagnetic BGA with the large size has never been successfully prepared in any kinds of Fe-based ferromagnetic BGA systems reported up to date because of the low GFA.

By using the $[(Fe_{0.6}Co_{0.3}Ni_{0.1})_{0.75}B_{0.2}Si_{0.05}]_{95}Nb_4Zr_1$ glassy alloy rod with a diameter of 2 mm, we measured mechanical properties by compressive test. Figure 6 shows the compressive stress-strain curves at a strain rate of 5×10^{-4} s^{-1}. The compressive stress-strain curve of the $[(Fe_{0.6}Co_{0.3}Ni_{0.1})_{0.75}B_{0.2}Si_{0.05}]_{96}Nb_4$ glassy alloy rod is also shown for comparison. The glassy alloy exhibits a superhigh

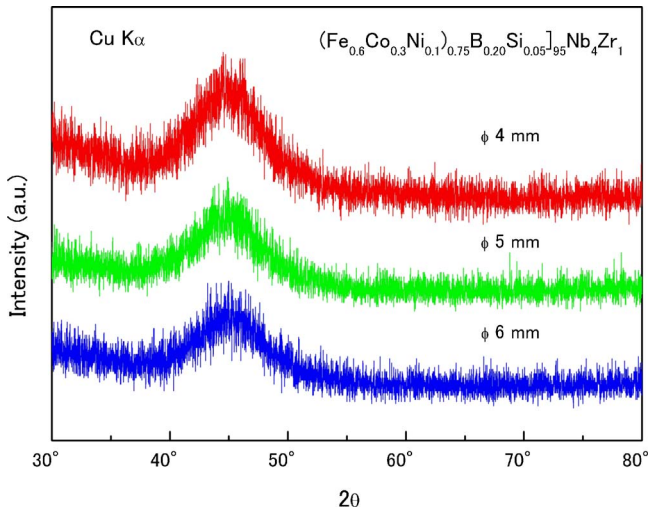

FIG. 5. (Color online) XRD patterns of the cast $[(Fe_{0.6}Co_{0.3}Ni_{0.1})_{0.75}B_{0.2}Si_{0.05}]_{95}Nb_4Zr_1$ rods with diameters of 4, 5, and 6 mm.

σ_f of 4180 MPa and elastic deformation up to a strain of about 0.02. Although no distinguished plastic deformation can be seen, the yield behavior can be clearly observed from the stress-strain curve, as the curve begins to deviate from linear. In addition, it is also seen that the sample undergoes a slight serrated deformation before final fracture. Figure 7 shows the macroscopic compressive fracture morphologies of the $[(Fe_{0.6}Co_{0.3}Ni_{0.1})_{0.75}B_{0.2}Si_{0.05}]_{95}Nb_4Zr_1$ glassy alloy rod. The fracture surface consists of a number of fracture zones and their planes appear to be declined by about 55°–90° to the direction of applied load, as shown in Fig. 7(a). The fracture behavior is different from the shear failure features[36–38] for Zr-, Cu-, and Ni-based BGAs where the fracture occurs nearly along the maximum shear stress plane which is declined by about 45° to the direction of applied load but nearly the same with the previous results of Fe-based BGAs.[13,39] For some Mg-, Co-, and Ti-based metallic glasses, it was found that they often failed in a fragmentation mode or distensile fracture[40–45] rather than in the conventional shear fracture mode.[46–49] Figure 7(b) shows the top view of the fracture surface. The fracture surface does not

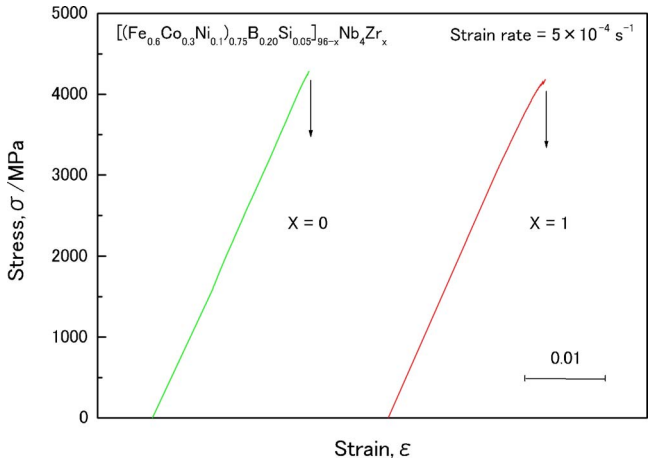

FIG. 6. (Color online) Compressive stress-strain curves of $[(Fe_{0.6}Co_{0.3}Ni_{0.1})_{0.75}B_{0.2}Si_{0.05}]_{96}Nb_4$ and $[(Fe_{0.6}Co_{0.3}Ni_{0.1})_{0.75}B_{0.2}Si_{0.05}]_{95}Nb_4Zr_1$ glassy alloy rods with a diameter of 2 mm.

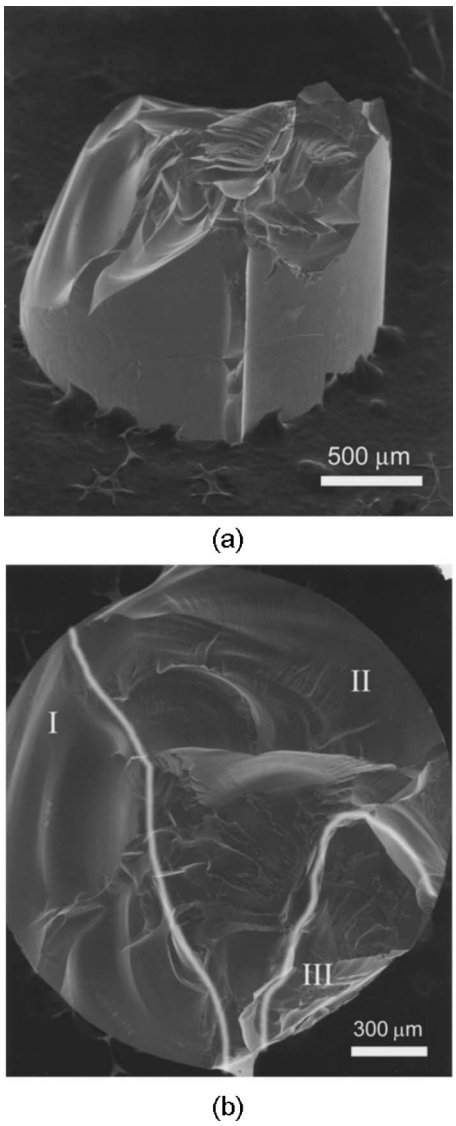

FIG. 7. SEM images revealing the compressive fracture feature of $[(Fe_{0.6}Co_{0.3}Ni_{0.1})_{0.75}B_{0.2}Si_{0.05}]_{95}Nb_4Zr_1$ glassy alloy rod. (a) Fracture of the compressive specimen. (b) Top view of the fracture surface.

exhibit shear stress plane, and three distinct regions marked as I, II, and III can be clearly seen. Region I shows a distinct cleavagelike fracture character. Region II exhibits a profound waterfall-like pattern, evidently demonstrating the branching, healing, and rebranching processes of the cracks along their propagation direction.[44] For region III, we observed it more carefully at high magnifications. As shown in Fig. 8(a), it is very interesting that both well developed patterns, i.e., vein—(areas 1, 2, and 4) and corelike (areas 3 and 5) patterns, can be clearly seen. As examples, areas 1 and 5 were further enlarged for observation. The enlarged images are shown in Figs. 8(b) and 8(c), respectively. One can obviously see the coexistence of the vein- and corelike patterns. The presence of corelike patterns provides experimental evidence of the local tensile stress present in the compressive fracture process.[46] Accordingly, these fracture patterns indicate that the sample experienced a rather complex stress state and obvious crack bifurcation prior to catastrophic failure, leading to the sample subjected to the serrated deformation before

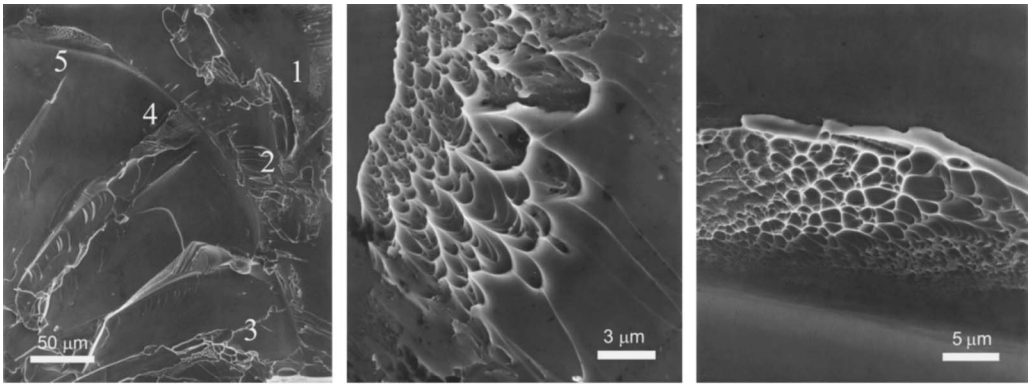

FIG. 8. SEM images showing region III shown in Fig. 7(b) at higher magnifications. (a) Enlarged image of region III shown in Fig. 7(b). (b) Enlarged image of area 1 as marked in (a). (c) Enlarged image of area 5 as marked in (a).

final fracture, which will be discussed later for better understanding the competition processes between shear and fragmentation mechanisms during compression of the Fe-based metallic glass.

Besides the superhigh σ_f, the $[(Fe_{0.6}Co_{0.3}Ni_{0.1})_{0.75}B_{0.2}Si_{0.05}]_{95}Nb_4Zr_1$ glassy alloy also exhibits good soft-magnetic properties, i.e., high I_s of 1.2 T and low H_c of 2 A/m. Figure 9 shows its frequency dependence of the permeability under a field of 1 A/m. As shown in the figure, the glassy alloy exhibits a high μ_e of 16 700 at 1 kHz combined with a high stability against the increase of frequency. Although μ_e decreases suddenly at about 25 kHz, it keeps a high value of 9500 even at 100 kHz. The origin of the excellent soft-magnetic properties can be attributed to the low number density of the domain-wall pinning sites,[50] resulting from the high degree of amorphicity and structural homogeneity proceeding from the high GFA of this Fe-CoNiBSiNbZr BGA.[51] It is therefore concluded that the Fe-CoNiBSiNbZr ferromagnetic BGA possesses simultaneously a high GFA, superhigh σ_f, rather high I_s, high T_C, low H_c, and high μ_e.

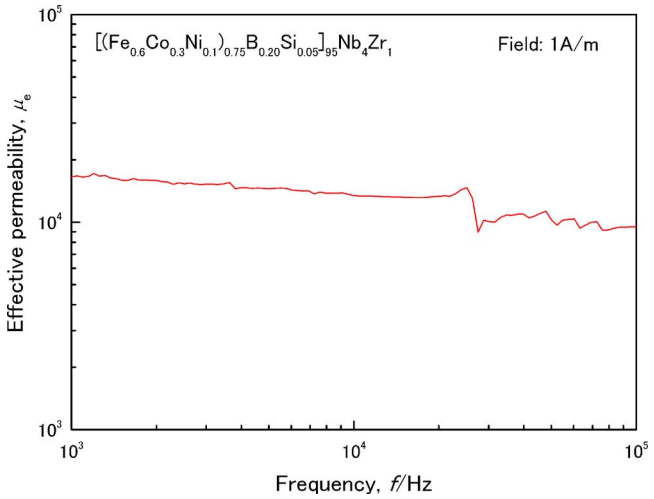

FIG. 9. (Color online) Effective permeability as a function of applied field frequency for the $[(Fe_{0.6}Co_{0.3}Ni_{0.1})_{0.75}B_{0.2}Si_{0.05}]_{95}Nb_4Zr_1$ glassy alloy annealed for 300 s at a temperature of T_g-50 K.

IV. DISCUSSION

First, we discuss the reason why only 1 at. % Zr addition is effective in improving the GFA. It is well known that large negative mixing enthalpies between the constituent elements lead to a highly stable supercooled liquid.[29] The mixing enthalpies between Zr and Fe, Co, Ni, B, or Si atomic pairs are −26, −41, −49, −56, and −67 kJ/mol, respectively, and they are larger than those between Nb and Fe, Co, Ni, B, or Si atomic pairs, which are −16, −25, −30, −39, and −39 kJ/mol, respectively.[52] However, the thermal stability of the supercooled liquid in this alloy system does not increase with increasing Zr content. Just 1 at. % Zr addition is effective in improving it, as shown in Figs. 1 and 2. It has been pointed out by Chen *et al.* that electrons could transfer from the metalloid elements, such as B and Si, fill the *d* shells of transition metal elements, such as Fe and Co, and then *s-d* hybrid bonding is formed.[53] The elastic moduli of Fe- and Co-based glassy alloys could be increased with metalloid addition, resulting from the strong interaction between the metal and metalloid atoms through *s-d* hybrid bonding.[54] In this study, Nb holds one 5*s* electron, but B, Si, and Zr hold two 2*s*, 3*s*, and 5*s* electrons, respectively. It is considered that one 5*s* electron is more active than those of two 2*s*, 3*s*, and 5*s* electrons, because the energy level of a pair of *s* electrons with inverse spin direction is much lower than that of one *s* electron. So the 5*s* electrons from Nb atoms would move more easily compared with those 2*s*, 3*s*, and 5*s* electrons from B, Si, and Zr atoms. Therefore, it is considered that the *s-d* hybrid bonding nature could become stronger by adding small amounts of Zr (only 1 at. % in this study), as Zr could supply *s* electrons. But the *s-d* hybrid bonding nature would become weaker with further increasing Zr content, because a large amount of Zr addition will decrease the fraction of 5*s* electrons with good activity from Nb atoms, leading to the decrease of the thermal stability of the supercooled liquid.

On the other hand, the atomic radii of Fe, Co, Ni, Nb, B, and Si are 0.124, 0.125, 0.125, 0.143, 0.09, and 0.117 nm, respectively.[55] Only Zr atom holds the largest atomic radius, which is 0.162 nm.[55] Although Poon *et al.* have pointed out that the large (*L*) and small (*S*) atoms could form a strong

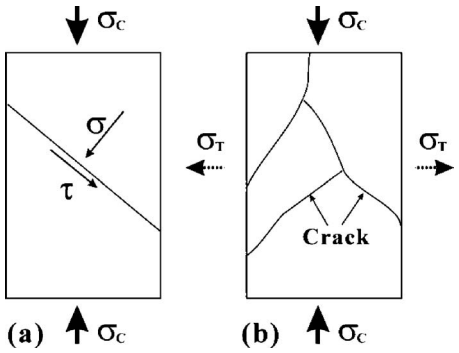

FIG. 10. Illustration of fracture processes of the Fe-based metallic glassy samples under compression: (a) the shear stress distribution on the shear plane and (b) fragmentation processes of the sample due to the lateral tensile stress.

L-S percolating network or reinforced "backbone" in the amorphous structure,[56] the significant difference in the atomic radii may cause the large strain between the atomic pairs. Thus, in this study, except for the decrease of the *s-d* hybrid bonding, another reason for the further increase of Zr content of over 1 at. % causing the decrease of the bonding nature could be attributed to the large strain between the atomic pairs. Therefore, it is considered that 1 at. % Zr addition is optimum in increasing the bonding nature of the networklike structure, resulting in enhancing the stability of the supercooled liquid, which suppresses crystallization. As to precipitate the $Fe_{23}B_6$-type phase, destroying the strong bonding nature is necessary before long-range atomic rearrangements of constituent elements, which results in the further increasing difficulty for the $(Fe,Co)_{23}B_6$ phase precipitation. Consequently, the synergism effects of *s-d* hybrid bonding and optimum *L-S* backbone lead to the highly stable supercooled liquid, which enables us to cast successfully Fe-based ferromagnetic BGAs with large diameters in the range up to 6 mm. It is noted that the alloy with 2 at. % Zr addition is the closest to the eutectic point in this alloy system as shown in Fig. 4, but this alloy does not exhibit the largest GFA, which cannot be cast into a glassy alloy rod with a diameter of 6 mm. The reason can be attributed to the bonding nature of the networklike structure, which is weaker than that of the 1 at. % Zr-containing alloy. Thus, it is suggested that the thermal stability of the supercooled liquid is the most important factor for preparing the large size BGA.

The fracture behavior during compression of the Fe-based metallic glass is very complicated as described earlier. It is well known that there exist two stresses, i.e., shear stress and normal stress, on any shear plane of a metallic glass sample subjected to a compressive load,[46–48] as illustrated in Fig. 10(a). If the critical shear strength τ_0 of the glassy sample is lower than the half of the compressive strength σ_C, i.e., $\tau_0 < \sigma_C/2$, the shear band will initiate and propagate approximately along the maximum shear stress plane, leading to the final shear failure, which can be widely observed in many Zr-, Cu-, and Ni-based BGA samples under compression.[36–38,46–49] However, if the critical shear strength τ_0 of the glassy sample is considerably higher than the half of the compressive strengths σ_C, i.e., $\tau_0 \geqslant \sigma_C/2$, it will be extremely difficult to stimulate the formation of the shear band. In this case, the metallic glass with very high critical shear strength τ_0 will have to fail in another mode rather than in the conventional shear fracture. Previously, we have defined a parameter, $\alpha = \tau_0/\sigma_0$, as fracture mode factor, where σ_0 is the critical cleavage fracture strength.[48] Therefore, the metallic glass failure in a fragmentation mode should have a relatively high fracture mode factor $\alpha = \tau_0/\sigma_0$ in comparison with those metallic glasses in a shear failure mode[49] because their critical shear strength τ_0 is very high. During compression deformation, according to Hook's law, the uniaxial compressive stress σ_C and compressive elastic strain ε_C will have the following relation, i.e.,

$$\sigma_C = E\varepsilon_C, \tag{1}$$

where, E is Young's modulus. When the metallic glass sample has a compressive elastic strain ε_C, there must be a lateral tensile elastic strain ε_T due to Poisson's effect; here, the two elastic strains ε_T and ε_C satisfy the rule

$$\nu = \varepsilon_T/\varepsilon_C, \tag{2}$$

where ν is Poisson's ratio. At the lateral tensile elastic strain ε_T, there must be a lateral tensile stress σ_T applied to the metallic glassy sample, i.e.,

$$\sigma_T = E\varepsilon_T = \nu\sigma_C. \tag{3}$$

This indicates that the lateral tensile stress σ_T is proportional to the compressive stress σ_C. When the lateral tensile stress σ_T is higher than the critical cleavage strength σ_0 of the metallic glass, i.e., $\sigma_T > \sigma_0$, multiple cleavage fracture will inevitably occur, as illustrated in Fig. 10(b), resulting in a fragmentation fracture feature [see Figs. 7(a) and 7(b)]. Based on the comparison above, one can get the following relations, i.e.,

$$\sigma_0 \leqslant \sigma_T = \nu\sigma_C, \tag{4}$$

and

$$\tau_0 \geqslant \sigma_C/2. \tag{5}$$

Therefore, from Eqs. (4) and (5), it is easy to calculate the fracture mode factor as below,

$$\alpha = \tau_0/\sigma_0 \geqslant 1/2\nu. \tag{6}$$

Assuming that Poisson's ratio is about 1/3, the fracture mode factor should be higher than 1.5, i.e., $\alpha = \tau_0/\sigma_0 \geqslant 1.5$. Just because of the very high fracture mode factor,[48] such kinds of metallic glasses, for example, Mg-, Co-, and Fe-based amorphous alloys, often fail either in a fragmentation mode or in a distensile fracture mode under compressive loading.[39–45] The cleavage fracture feature can be clearly seen in the fracture surfaces in Figs. 7 and 8.

V. SUMMARY

We synthesized an Fe-based ferromagnetic glassy alloy $[(Fe_{0.6}Co_{0.3}Ni_{0.1})_{0.75}B_{0.2}Si_{0.05}]_{95}Nb_4Zr_1$ with high glass-forming ability that can be cast into bulk glassy alloy rods with the diameters in the range up to 6 mm, superhigh fracture strength of 4180 MPa, rather high saturation magnetization of 1.1 T, low coercive force of 2 A/m, and high initial permeabilities of 16 700 and 9500 at 1 and 100 kHz, respec-

tively, under a field of 1 A/m. The strong bonding nature of the networklike structure resulting from only 1 at. % Zr addition leads to the high glass-forming ability and superhigh fracture strength. The excellent soft-magnetic properties are attributed to the high degree of amorphicity and structural homogeneity proceeding from the high glass-forming ability. Besides, this Fe-based bulk glassy alloy exhibits yield behavior before final fracture, although the superhigh critical shear strength leads this Fe-based bulk glassy alloy to fail in a fragmentation mode. In general, this $[(Fe_{0.6}Co_{0.3}Ni_{0.1})_{0.75}B_{0.2}Si_{0.05}]_{95}Nb_4Zr_1$ ferromagnetic bulk glassy alloy simultaneously exhibiting high glass-forming ability, superhigh fracture strength and excellent soft-magnetic properties is promising for applications as not only functional but also structural materials in the near future.

ACKNOWLEDGMENTS

This work was financially supported by the Grant-in-Aid for Scientific Research (Basic Research C) of the Japan Society for the Promotion of Science (JSPS) under Grant No. 18560670 and the National Natural Science Foundation of China (NNSFC) under Grant Nos. 50401019 and 50625103 as well as the "Hundred of Talents Project" by the Chinese Academy of Sciences.

[1]H. Fujimori, T. Masumoto, Y. Obi, and M. Kikuchi, Jpn. J. Appl. Phys. **13**, 1889 (1974).
[2]T. Egami, P. J. Flanders, and C. D. Graham, Jr., Appl. Phys. Lett. **26**, 128 (1975).
[3]R. C. O'Handley, R. Hasegawa, R. Ray, and C. P. Chou, Appl. Phys. Lett. **29**, 330 (1976).
[4]R. W. Cahn, in *Rapidly Solidified Alloys*, edited by H. H. Liebermann (Dekker, New York, 1993), pp. 1–15.
[5]A. Inoue and J. S. Gook, Mater. Trans., JIM **36**, 1180 (1995).
[6]A. Inoue, Y. Shinohara, and J. S. Gook, Mater. Trans., JIM **36**, 1427 (1995).
[7]T. D. Shen and R. B. Schwarz, Appl. Phys. Lett. **75**, 49 (1999).
[8]A. Inoue, A. Takeuchi, and B. L. Shen, Mater. Trans. **42**, 970 (2001).
[9]B. L. Shen and A. Inoue, Mater. Trans. **43**, 1235 (2002).
[10]A. Inoue, B. L. Shen, H. Koshiba, H. Kato, and A. R. Yavari, Nat. Mater. **2**, 661 (2003).
[11]V. Ponnambalam, S. J. Poon, and G. J. Shiflet, J. Mater. Res. **19**, 1320 (2004).
[12]Z. P. Lu, C. T. Liu, J. R. Thompson, and W. D. Porter, Phys. Rev. Lett. **92**, 245503 (2004).
[13]A. Inoue, B. L. Shen, and C. T. Chang, Acta Mater. **52**, 4093 (2004).
[14]B. L. Shen, and A. Inoue, J. Phys.: Condens. Matter **17**, 5647 (2005).
[15]S. H. Sheng, C. L. Ma, S. J. Pang, and T. Zhang, Mater. Trans. **46**, 2949 (2005).
[16]K. Amiya and A. Inoue, Mater. Trans. **47**, 1615 (2006).
[17]P. Pawlik, H. A. Davies, and M. R. J. Gibbs, Appl. Phys. Lett. **83**, 2775 (2003).
[18]B. L. Shen, A. Inoue, and C. T. Chang, Appl. Phys. Lett. **85**, 4911 (2004).
[19]W. H. Wang, M. X. Pan, D. Q. Zhao, Y. Hu, and H. Y. Bai, J. Phys.: Condens. Matter **16**, 3719 (2004).
[20]R. B. Schwarz, T. D. Shen, U. Harms, and T. Lillo, J. Magn. Magn. Mater. **283**, 223 (2004).
[21]C. Y. Lin, H. Y. Tien, and T. S. Chin, Appl. Phys. Lett. **86**, 162501 (2005).
[22]J. M. Park, J. S. Park, D. H. Kim, J. H. Kim, and E. Fleury, J. Mater. Res. **21**, 1019 (2006).
[23]C. T. Chang, B. L. Shen, and A. Inoue, Appl. Phys. Lett. **88**, 011901 (2006).
[24]B. L. Shen, M. Akiba, and A. Inoue, Appl. Phys. Lett. **88**, 131907 (2006).
[25]C. T. Chang, B. L. Shen, and A. Inoue, Appl. Phys. Lett. **89**, 051912 (2006).
[26]S. J. Pang, T. Zhang, K. Asami, and A. Inoue, Acta Mater. **50**, 489 (2002).
[27]A. Inoue and B. L. Shen, Mater. Trans. **43**, 2350 (2002).
[28]A. Inoue, B. L. Shen, and T. Takeuchi, Mater. Trans. **47**, 1275 (2006).
[29]A. Inoue, Acta Mater. **48**, 279 (2000).
[30]D. V. Louzguine, S. Sobu, and A. Inoue, Appl. Phys. Lett. **85**, 3758 (2004).
[31]A. Inoue and B. L. Shen, Adv. Mater. (Weinheim, Ger.) **16**, 2189 (2004).
[32]B. L. Shen, M. Akiba, and A. Inoue, Phys. Rev. B **73**, 104204 (2006).
[33]B. L. Shen, C. T. Chang, T. Kubota, and A. Inoue, J. Appl. Phys. **100**, 013515 (2006).
[34]M. Imafuku, S. Sato, H. Kosiba, E. Matubara, and A. Inoue, Mater. Trans., JIM **41**, 1526 (2000).
[35]M. Imafuku, C. F. Li, M. Matsushita, and A. Inoue, Jpn. J. Appl. Phys., Part 1 **41**, 219 (2002).
[36]A. Inoue and T. Zhang, Mater. Trans., JIM **36**, 1184 (1995).
[37]A. Inoue, W. Zhang, T. Zhang, and K. Kurosaka, Acta Mater. **49**, 2645 (2001).
[38]T. Zhang and A. Inoue, Mater. Trans. **43**, 708 (2002).
[39]M. Stoica, J. Eckert, S. Roth, Z. F. Zhang, L. Schultz, and W. H. Wang, Intermetallics **13**, 764 (2005).
[40]Y. K. Xu, H. Ma, J. Xu, and E. Ma, Acta Mater. **53**, 1857 (2005).
[41]X. K. Xi, D. Q. Zhao, M. X. Pan, W. H. Wang, Y. Wu, and J. J. Lewandowski, Phys. Rev. Lett. **94**, 125510 (2005).
[42]Z. F. Zhang, H. Zhang, B. L. Shen, A. Inoue, and J. Eckert, Philos. Mag. Lett. **86**, 643 (2006).
[43]Z. F. Zhang, F. F. Wu, W. Gao, J. Tan, Z. G. Wang, M. Stoica, J. Das, J. Eckert, B. L. Shen, and A. Inoue, Appl. Phys. Lett. **89**, 251917 (2006).
[44]J. Shen, W. Z. Lian, and J. F. Sun, Appl. Phys. Lett. **89**, 121908 (2006).
[45]Z. F. Zhang, G. He, and J. Eckert, Philos. Mag. **85**, 897 (2005).
[46]Z. F. Zhang, J. Eckert, and L. Schultz, Acta Mater. **51**, 1167 (2003).
[47]Z. F. Zhang, G. He, J. Eckert, and L. Schultz, Phys. Rev. Lett. **91**, 045505 (2003).
[48]Z. F. Zhang and J. Eckert, Phys. Rev. Lett. **94**, 094301 (2005).
[49]Z. F. Zhang and J. Eckert, Adv. Eng. Mater. **9**, 143 (2007).
[50]T. Bitoh, A. Makino, and A. Inoue, J. Appl. Phys. **99**, 08F102 (2006).
[51]A. Inoue, Mater. Sci. Eng., A **304–306**, 1 (2001).
[52]F. R. De Boer, R. Boom, W. C. M. Mattens, and A. R. Miedema, and A. K. Niessen, in *Cohesion in Metals*, edited by F. R. De Boer and D. G. Pettifor (North-Holland, Amsterdam, 1989), pp. 217–403.
[53]H. S. Chen, J. T. Krause, and E. Coleman, J. Non-Cryst. Solids **18**, 157 (1975).
[54]H. S. Chen, J. Appl. Phys. **49**, 462 (1978).
[55]*Metals Databook* (The Japan Institute of Metals, Maruzen, Tokyo, 2004), p. 8.
[56]S. J. Poon, G. J. Shiflet, F. Q. Guo, and V. Ponnambalam, J. Non-Cryst. Solids **317**, 1 (2003).